Article

Cell Reports

Entosis Is Induced by Glucose Starvation

Graphical Abstract

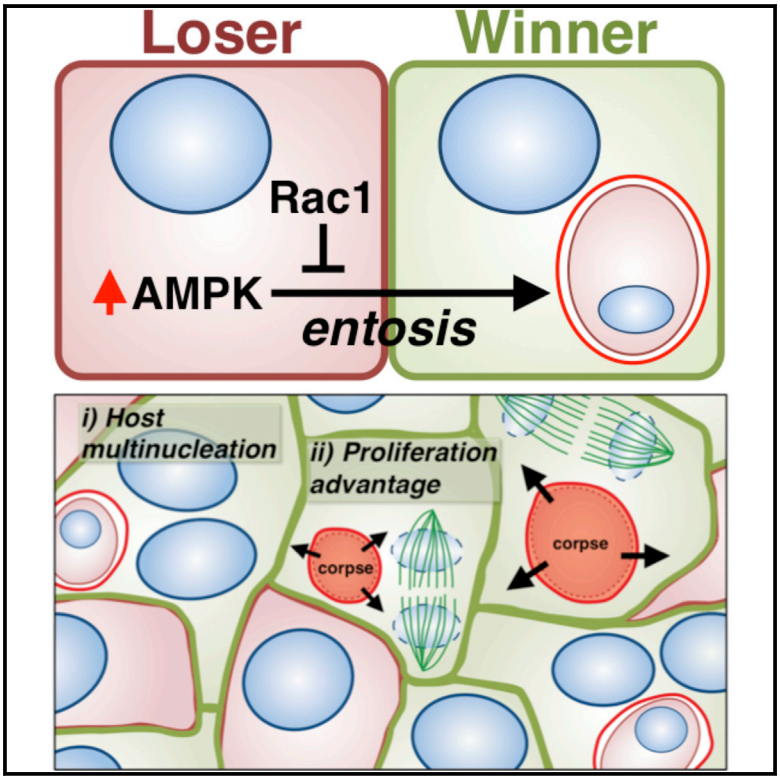

Authors

Jens C. Hamann, Alexandra Surcel, Ruoyao Chen, Carolyn Teragawa, John G. Albeck, Douglas N. Robinson, Michael Overholtzer

Correspondence

overhom1@mskcc.org

In Brief

Entosis has been shown to occur in human cancers and promotes cell competition. Hamann et al. now show that nutrient deprivation, in the form of glucose withdrawal, induces entosis to support the outgrowth of winner cells that feed off of losers.

Highlights

- Glucose starvation induces entosis in cancer cells
- AMPK regulates loser cell behavior by altering cell mechanics
- Entosis supports winner cell proliferation
- Long-term starvation selects for winner cells

Hamann et al., 2017, Cell Reports *20*, 201–210
July 5, 2017
http://dx.doi.org/10.1016/j.celrep.2017.06.037

Cell Reports
Article

Entosis Is Induced by Glucose Starvation

Jens C. Hamann,[1,2] Alexandra Surcel,[3] Ruoyao Chen,[1,4] Carolyn Teragawa,[5] John G. Albeck,[5] Douglas N. Robinson,[3] and Michael Overholtzer[1,6,*]
[1]Cell Biology Program, Memorial Sloan Kettering Cancer Center, New York, NY 10065, USA
[2]Louis V. Gerstner, Jr. Graduate School of Biomedical Sciences, Memorial Sloan Kettering Cancer Center, New York, NY 10065, USA
[3]Department of Cell Biology, Johns Hopkins University School of Medicine, Baltimore, MD 21205, USA
[4]BCMB Allied Program, Weill Cornell Medical College, New York, NY 10065, USA
[5]Department of Molecular and Cellular Biology, University of California, Davis, Davis, CA 95616, USA
[6]Lead Contact
*Correspondence: overhom1@mskcc.org
http://dx.doi.org/10.1016/j.celrep.2017.06.037

SUMMARY

Entosis is a mechanism of cell death that involves neighbor cell ingestion. This process occurs in cancers and promotes a form of cell competition, where winner cells engulf and kill losers. Entosis is driven by a mechanical differential that allows softer cells to eliminate stiffer cells. While this process can be induced by matrix detachment, whether other stressors can activate entosis is unknown. Here, we find that entosis is induced in adherent cells by glucose withdrawal. Glucose withdrawal leads to a bimodal distribution of cells based on their deformability, where stiffer cells appear in a manner requiring the energy-sensing AMP-activated protein kinase (AMPK). We show that loser cells with high levels of AMPK activity are eliminated by winners through entosis, which supports winner cell proliferation under nutrient-deprived conditions. Our findings demonstrate that entosis serves as a cellular response to metabolic stress that enables nutrient recovery through neighbor cell ingestion.

INTRODUCTION

Programmed cell death is essential for promoting proper tissue development and homeostasis and for inhibiting the development of diseases such as cancer. While programmed cell death was once considered to occur only by apoptosis, many alternative forms of cell death have recently been identified that may also regulate cell turnover in a context-dependent manner. For example, regulated forms of necrosis (necroptosis [Degterev et al., 2005] and ferroptosis [Dixon et al., 2012]) and autophagic cell death are now known to contribute to cell death induced by viral infection (Linkermann and Green, 2014) and nutrient deprivation (Gao et al., 2015; Liu et al., 2013) and to programmed cell death during development (Nelson et al., 2014).

In addition to these regulated forms of cell death, other alternative forms have been reported that may represent yet-additional programmed mechanisms that eliminate cells in certain contexts (Galluzzi et al., 2012). Among these, entosis is a mechanism that targets cells for death following their engulfment by neighboring cells (Overholtzer et al., 2007). Entotic cells are killed non-cell autonomously by engulfing cells through autophagy protein-dependent lysosomal digestion (Florey et al., 2011). Entosis occurs in human cancers, and we have shown that it inhibits transformed growth by inducing cell death. However, this process also promotes the development of aneuploidy in host cells (Krajcovic et al., 2011) and facilitates nutrient recovery by engulfing cells that could function to promote tumor progression (Krajcovic et al., 2013). Recently, we demonstrated that entosis acts as a form of cell competition, where the engulfment of loser cells by neighboring winners can promote clonal selection within heterogeneous tumor cell populations (Sun et al., 2014b). Competition is driven by a mechanical differential between softer (reduced elasticity) cells and stiffer cells, where stiffer cells are eliminated by softer winners (Sun et al., 2014b).

While recent studies have elucidated consequences of entosis on cell populations, the signals that could promote this process remain poorly characterized, with a lack of suitable matrix adhesion as the only clear known inducer of entosis (Overholtzer et al., 2007). As entosis, like autophagy, can allow for nutrient recovery that supports cell survival and proliferation under conditions of starvation (Krajcovic et al., 2013), we considered if entosis might also be induced by nutrient deprivation. Here, we identify glucose starvation, acting through an AMP-activated protein kinase (AMPK)-dependent mechanical differential, as a potent activator of entosis in matrix-adherent cancer cells.

RESULTS

Entosis Is Induced in Cancer Cells by Glucose Withdrawal

We previously reported that cell engulfment by entosis allows cells to recover nutrients that can support cell survival and proliferation under conditions of amino acid deprivation (Krajcovic et al., 2013). However, amino acid withdrawal did not induce high levels of entosis, prompting us to examine whether other forms of nutrient starvation could induce high rates of neighbor cell ingestion. To identify potential entotic triggers, we cultured MCF-7 human breast tumor cells, which undergo high levels of entosis in matrix-detached conditions, in various nutrient-depleted conditions.

After 72 hr in medium containing low serum, no glucose, and no amino acids, neighboring cells engulfed each other at high rates, with more than 30% of adherent cells containing an average of two engulfed neighbors (Figure 1A). Often, more complicated cell structures were observed, with three or more cells involved in sequential engulfments (Figures 1Ai and 1Aii), similar to the entotic structures reported in matrix-detached cultures. Interestingly, the withdrawal of glucose from growth medium, unlike starvation for other nutrients, was sufficient to induce a high level of cell engulfment (Figure 1A), and re-addition of D-glucose to glucose-free medium completely rescued this effect (Figure 1C). Glucose starvation therefore appears to be a primary trigger of cell engulfment.

Entotic cell engulfment is known to involve cell contractility of internalizing cells, regulated by RhoA and Rho-kinase (ROCK) signaling, and cell-cell adhesions, mediated by E-cadherin. To determine if cell engulfment induced by glucose starvation occurs by entosis, we examined cells for the presence of these characteristics. First, activated myosin II, indicated by phosphorylation of myosin light chain 2 on the ROCK-dependent site serine 19 (P-MLC^{S19}), was localized at the cortex of the internalizing cells, as reported (Sun et al., 2014a) (Figure 1B). Further, treatment with Y-27632, an inhibitor of ROCK and a potent entosis inhibitor, also completely blocked cell engulfment induced by glucose withdrawal (Figure 1C). Second, the cell-cell adhesion protein β-catenin localized at the interface between internalizing and engulfing cell pairs, consistent with a cell-cell-adhesion-based mechanism of uptake (Figure 1B). Accordingly, disruption of E-cadherin in MCF-7 cells, by CRISPR/Cas9-mediated gene editing, significantly inhibited cell engulfment due to glucose withdrawal, which was rescued by exogenous expression of E-cadherin-GFP (Figures 1D and S1A). We also examined whether MDA-MB-231 breast cancer cells, which are E-cadherin deficient and do not normally undergo entosis (Sun et al., 2014a), could undergo cell engulfment in response to glucose deprivation. MDA-MB-231 cells showed no evidence of engulfment in either glucose-starved or full media conditions (Figure 1E). However, upon expression of exogenous E-cadherin, MDA-MB-231 cells exhibited a significant rate of cell engulfment with glucose starvation (Figure 1E). To examine whether this effect was unique to cancer cells or common among non-transformed cells as well, we cultured a non-transformed mammary epithelial cell line (MCF-10A) in glucose-free conditions for multiple days and found that levels of entosis within the culture also increased, although to a lower extent than in MCF-7 cells (Figures S1B and S1C). We therefore conclude that glucose starvation is an inducer of entosis in breast cancer cells and non-transformed mammary epithelial cells.

Entotic Cell Death Is Increased in Glucose-Starved Conditions

Entosis leads to the death of internalized cells through a non-apoptotic mechanism that involves lipidation of the autophagy protein LC3 onto entotic vacuoles (Florey et al., 2011). Typically, 50%–70% of internalized cells undergo death by this mechanism within a 24 hr period, while others (10%–20%) manage to escape from their hosts (Overholtzer et al., 2007; Florey et al., 2011). Interestingly, under conditions of glucose withdrawal, we noted that entotic cells died more rapidly after their engulfment and rarely escaped (Figure 2A). More than 60% of engulfed cells died within 5 hr after engulfment, compared to 10% of engulfed cells cultured in full media. Ten hours after engulfment was complete, more than 90% of internalized cells cultured in glucose-free media had undergone cell death, while only ~50% of engulfed cells grown in full media had died (Figure 2A). Like entotic cell deaths occurring in nutrient-rich conditions, those occurring in glucose-starved cultures involved lipidation of LC3 onto entotic vacuoles, and the frequency of cell death was reduced by knockdown of the autophagy protein Atg5 (Figures 2A, 2B, and S2A).

The Energy-Sensing Kinase AMPK Regulates Loser Cells during Glucose-Starvation-Induced Entosis

To identify the signaling mechanisms that might control glucose starvation-induced entosis, we considered AMPK, a well-known starvation-induced kinase that allows cells to respond to starvation stress by inducing autophagy (Yuan et al., 2013). Treatment with compound C, an inhibitor of AMPK (Zhou et al., 2001), as well as expression of dominant-negative isoforms of AMPK (AMPK-DN) (Mu et al., 2001; Young et al., 2016) inhibited entosis induction in the absence of glucose (Figures 3A, S3A, and S3B). Conversely, entosis was induced in nutrient-rich media by the induction of AMPK activity using two AMPK activators, the AMP analog 5-Aminoimidazole-4-carboxamide ribonucleotide (AICAR) (Sullivan et al., 1994) and the allosteric activator A-769662 (Göransson et al., 2007) (Figures 3A, S3A, and S3C), indicating that AMPK plays an important role in promoting this process.

To determine if AMPK activation occurs in winner or loser cells, we utilized a fluorescence resonance energy transfer (FRET)-based sensor (Tsou et al., 2011) to monitor temporal AMPK dynamics. Shortly before engulfment, we observed an increase in FRET-based fluorescence (indicating increased AMPK activity) within internalizing MCF-7 cells undergoing glucose-withdrawal-induced entosis (Figure 3B). This finding is consistent with previous reports of this sensor that showed similar fold increases in FRET signal upon glucose starvation (Banko et al., 2011; Tsou et al., 2011). We then co-cultured MCF-7 cells expressing AMPK-DN with control MCF-7 cells expressing GFP in the absence of glucose. While control mCherry-expressing MCF-7 cells were winners at ~50% frequency, MCF-7 cells expressing AMPK-DN were winner cells in ~75% of heterotypic entotic structures, consistent with the idea that AMPK acts within loser cells (Figures 3C and S3D). Interestingly, inhibition of AMPK, either by expression of AMPK-DN or treatment with compound C, or activation of AMPK by treatment with AICAR did not alter the rates of cell death once loser cells became internalized, suggesting the rapid rate of loser cell death observed in glucose-free conditions is independent of AMPK activity (Figures S2B and S2C).

We then tested whether glucose deprivation primarily promotes entosis by inducing loser cell status. We took advantage of our previous observation that expression of a constitutively active form of Rac1 (Rac1^{V12}, hereafter Rac1^{CA}-GFP) can inhibit cell uptake by blocking loser cell internalization while promoting

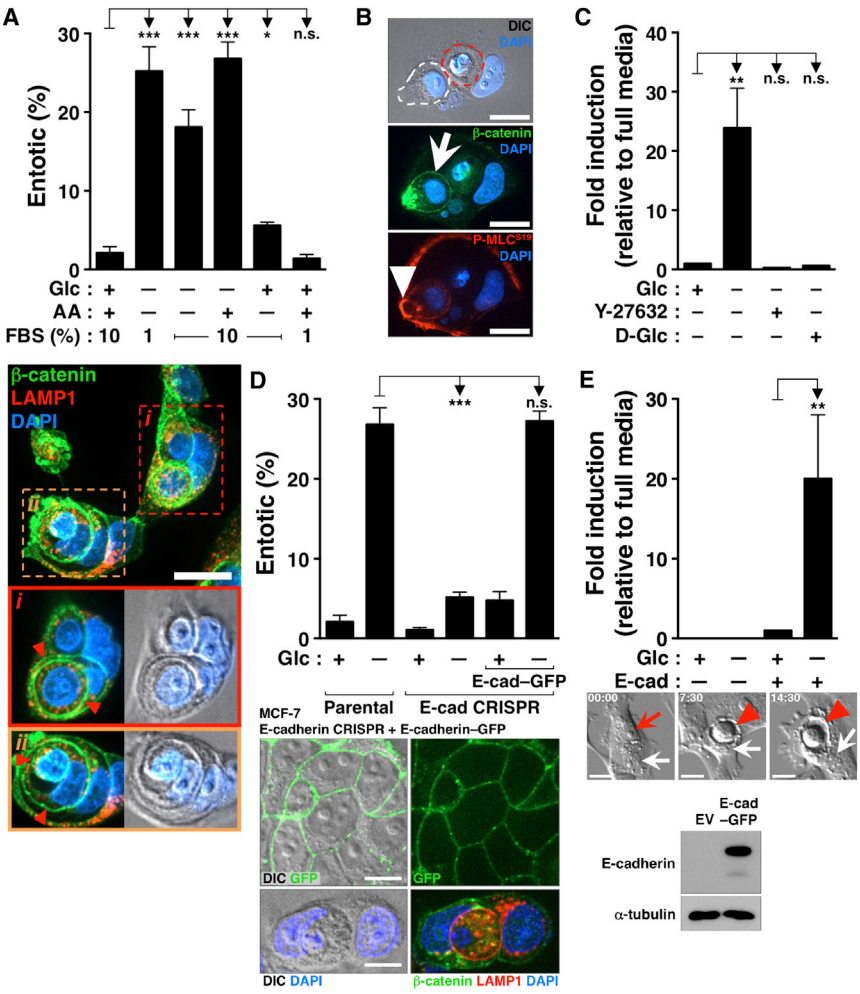

Figure 1. Glucose Starvation Induces Entosis in Breast Cancer Cell Lines

(A) Nutrient starvation causes engulfment. Graph shows the percentage of engulfment in MCF-7 cells grown in the indicated conditions for 72 hr, as determined by immunofluorescence. Glc, glucose; AA, amino acids; FBS, fetal bovine serum. Error bars depict mean ± SEM; data are from at least three independent experiments. Images show engulfed cell structures from a 72-hr glucose-starved culture. Immunostaining for β-catenin (green) and Lamp1 (red) and DAPI-stained nuclei (blue) are shown. Arrowheads show completed engulfments. Scale bar, 20 μm.

(B) Localization of cellular machinery required for entosis. Immunofluorescence image shows localization of phosphorylated myosin light chain (P-MLC^{S19}; red, arrowhead) in MCF-7 cells grown in glucose-free conditions for 72 hr. Cell-cell junctions are shown by β-catenin staining (green, arrow), and DAPI-stained nuclei are shown in blue. The white dashed line shows the outline of partial engulfment, while the red dashed line shows the engulfed corpse. Scale bars, 15 μm.

(C) Induction of engulfment is blocked by ROCK inhibition and readdition of glucose. Graph shows the quantification of engulfment over 72 hr, as determined by time-lapse microscopy. Error bars depict mean ± SEM; data are from at least three independent experiments.

(D) Loss of E-cadherin blocks entosis. Graph shows percentage of engulfment in parental MCF-7 cells, as well as E-cad CRISPR and E-cad CRISPR + E-cad-GFP cells, grown in the indicated media conditions for 72 hr, as determined by immunofluorescence. Error bars depict mean ± SEM; data are from at least three independent experiments. Representative images show expected plasma membrane localization of exogenous E-cadherin-GFP in MCF-7 E-cad CRISPR + E-cad-GFP cells (top row) and induction of entosis in these cells (bottom row). Immunostaining for β-catenin (green) and Lamp1 (red) and DAPI-stained nuclei (blue) is shown. Scale bars, 10 μm. See also Figure S1A.

(E) Engulfment is induced during glucose starvation in MDA-MB-231 cells expressing E-cadherin. Shown is the quantification of engulfment over 72 hr for MDA-MB-231 cells expressing either empty vector (EV) or E-cadherin-GFP, cultured in full or glucose-free media, as determined by time-lapse microscopy. Error bars depict mean ± SEM; data are from at least three independent experiments. A representative image sequence of MDA-MB-231 cells expressing E-cadherin-GFP undergoing engulfment is shown in glucose-free conditions. The red arrow shows a cell to be internalized before engulfment. White arrows show the host cell. The red arrowheads show engulfment. Time shown is in hours:minutes. Scale bars, 10 μm. Western blot shows expression of E-cadherin in parental and E-cadherin-GFP-expressing MDA-MB-231 cells.

winner cell behavior (Sun et al., 2014b). Rac1^{CA}-GFP expression completely blocked the induction of entosis in glucose-depleted conditions (Figure 3D), consistent with the model that glucose deprivation activates entosis by stimulating loser cell behavior through increased AMPK activity, and activation of Rac1 can override this signal.

Glucose Starvation Results in Changes in Cell Deformability

A differential in cell deformability (inverse elasticity) appears to be a requisite for entosis (Sun et al., 2014b). We therefore sought to determine if mechanical deformability is altered in glucose-starved cell populations using micropipette aspiration (MPA). Control cells display a monomodal distribution of deformability (Figure 4A). However, glucose-starved cells were distributed into a bimodal population based on their mechanical profiles, with cells exhibiting relatively more (low elastic modulus) or less (high elastic modulus) deformability (Figure 4A). The measured elastic modulus of the less deformable cell population that appeared upon glucose starvation was significantly higher than that of MCF-7 cells in nutrient-rich medium, suggesting this population could represent loser cells within the population, similar to what we observed previously (Sun et al., 2014b) (Figure 4C). To examine if AMPK plays a role in controlling the appearance of this population, we performed MPA with control and glucose-starved MCF-7 cells expressing AMPK-DN. After glucose starvation, the number of cells clustering into the high elasticity population was significantly reduced, suggesting that AMPK activity impacts loser cell behavior, in part, by altering cell deformability (Figure 4B).

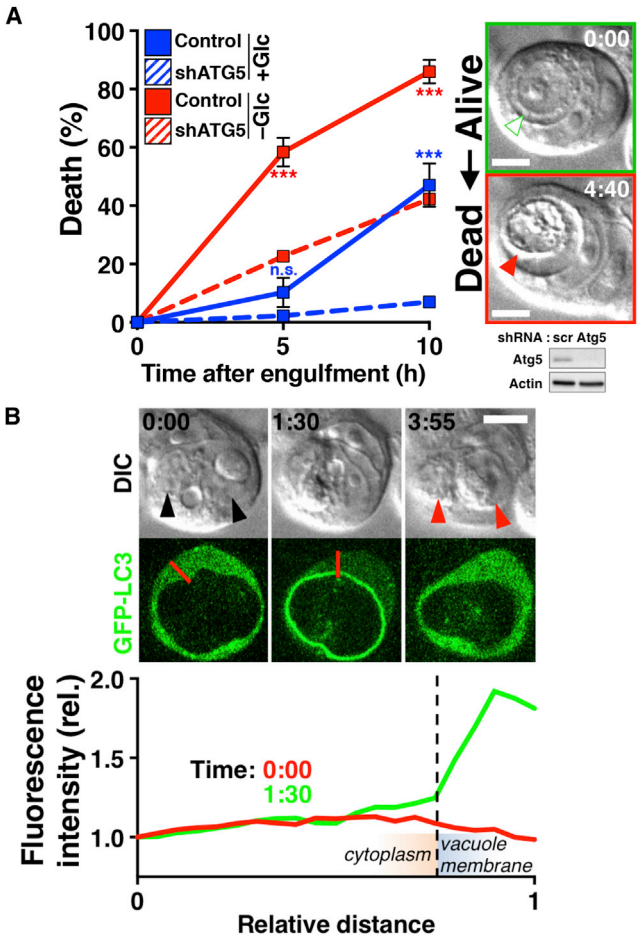

Figure 2. Glucose Starvation Increases Entotic Cell Death

(A) Entotic death rate of internalized cells increases during glucose starvation. Graph shows death rate of internalized cells within 10 hr after completed engulfment, as determined by the appearance of a vacuole within the host cell by DIC microscopy. Entotic death rates for cells cultured in full media (+Glc, blue lines) or glucose-free media (−Glc, red lines) in control MCF-7 cells (solid lines) and MCF-7 shATG5 cells (dashed lines) are shown. Error bars depict mean ± SEM; data are from at least three independent experiments, with n ≥ 40 entotic cell structures per experiment. p values according to two-way ANOVA multiple comparisons test. p values compare control and shATG5 cells in +Glc or −Glc media, respectively, and are color-coded accordingly. Western blot shows expression of Atg5 relative to actin in MCF-7 cells expressing a scrambled or Atg5-targeted shRNA. Images are representative of live and dead internalized cells as scored by DIC. The green and white arrowhead shows a live internalized cell ("alive"); the red arrowhead shows a morphologically dead cell inside the host cell vacuole ("dead"). Time shown is in hours:minutes. Scale bars, 10 μm. See also Figure S2A.

(B) Internalized cell death involves transient lipidation of LC3 (light chain 3) onto entotic vacuoles. Confocal time-lapse images of MCF-7 cells expressing GFP-LC3 cultured in glucose-free media. Black arrowheads show two live engulfed cells within a GFP-LC3-expressing host (one inner cell contains a corpse). Red arrowheads show death of both internalized cells ~4 hr after LC3 recruitment. Time shown is in hours:minutes. Scale bar, 10 μm. Graph shows relative GFP fluorescence intensity both before (0:00) and during (1:30) GFP-LC3 recruitment. The line used for the fluorescence intensity profile is shown in red.

Entosis Supports Proliferation in Nutrient-Limiting Conditions

We next examined the consequences of glucose-withdrawal-induced entosis on cell populations. We asked whether the ingestion and degradation of loser cells could provide winner cells with nutrients that support cell survival or proliferation during starvation, similar to what we have shown for amino acid starvation (Krajcovic et al., 2013). Indeed, even under stringent conditions of dual glucose and amino acid deprivation, cells that had ingested their neighbors proliferated 10-fold more frequently than control single-cell neighbors (Figures 5A and S4A). We further examined the effects of entosis in glucose-starved conditions over a longer time course. Over the first 72 hr of glucose starvation, the population size was significantly reduced by frequent cell deaths occurring with entotic, necrotic, or apoptotic morphologies, as quantified by time-lapse microscopy (Figures 5B and 5C). Following 72 hr, MCF-7 cells expressing E-cadherin exhibited a population doubling after 6 days of continued growth in the absence of glucose (Figure 5D). Conversely, cells lacking E-cadherin, which are deficient for entosis induction, had an impaired ability to grow under starvation conditions, despite reduced levels of cell death overall, and a slightly increased ability to proliferate under nutrient-replete conditions (Figures 5B and 5D; data not shown). Altogether, these data are consistent with a model that entosis induced by nutrient starvation supports the proliferation of winner cells under conditions of continued nutrient withdrawal.

Typically, entotic cell structures induce the generation of aneuploid cell lineages due to the failure of engulfing cells to divide properly (Krajcovic et al., 2011). Because most cell divisions occurring under starvation conditions involved entotic cell structures, we examined if nutrient withdrawal led to the appearance of multinucleated cells. Indeed, nutrient starvation induced a 5-fold increase in the percentage of cells exhibiting multinucleation (Figures 5E and S4B), suggesting that starvation can disrupt cell ploidy by inducing entosis.

To examine the properties of cancer cell populations selected by glucose starvation, we took advantage of our observation that MCF-7 cells could be grown in the absence of glucose for extended periods (MCF-7^{-Glc}). MCF-7^{-Glc} cells were selected in continuous culture for 36–78 days in the absence of glucose. We co-cultured MCF-7^{-Glc} cells with passage-matched parental starvation-naive MCF-7 cells (MCF-7^{parental}) and quantified winner and loser status of each cell population in heterotypic entotic cell structures. In glucose-free conditions, MCF-7^{-Glc} displayed a marked increase in winner cell activity (Figure 5F). Thus, cells continually grown in glucose-depleted conditions maintain altered characteristics that confer winner status when co-cultured with parental cells under starvation conditions. Consistent with AMPK controlling loser cell activity, selected cells also exhibited reduced AMPK activation, as well as lowered levels of P-MLC^{S19}, indicative of winner cells (Figure 5G).

Altogether, our data demonstrate that glucose starvation induces a high level of entosis in matrix-adherent breast cancer cell populations, in a manner controlled by AMPK activity in loser cells. Glucose starvation results in the emergence of a bimodal mechanical distribution of cells, where AMPK is required for the appearance of the less deformable subpopulation that we

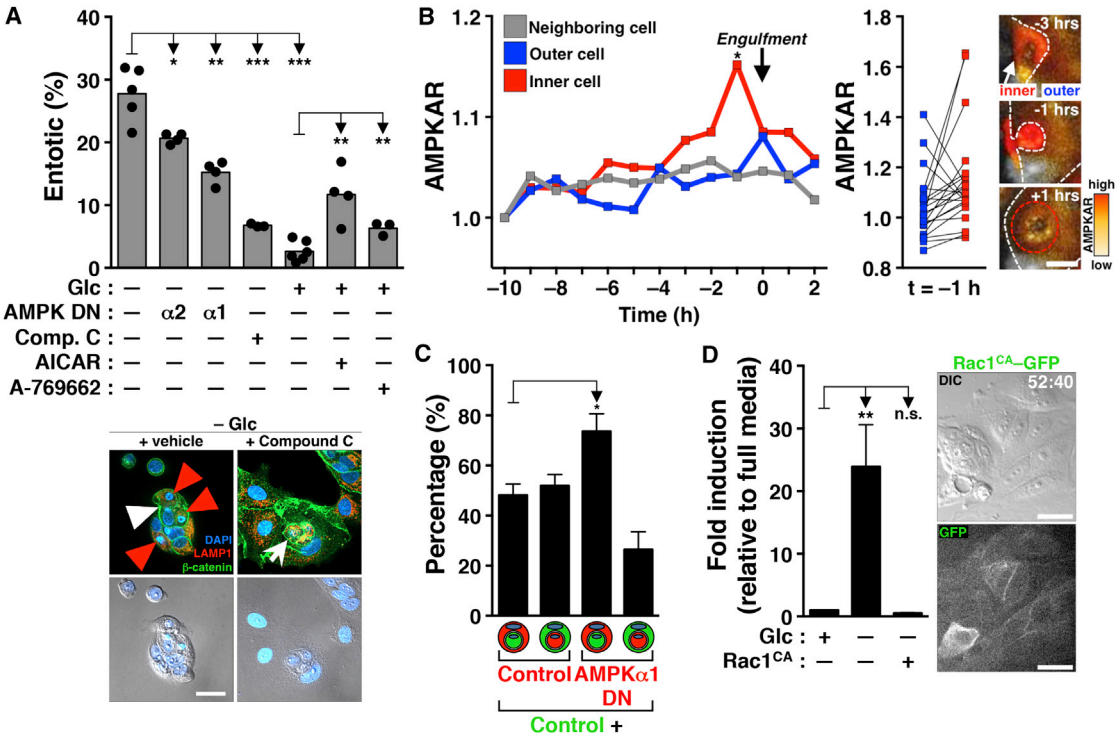

Figure 3. AMPK Regulates Loser Cells during Glucose-Starvation-Induced Entosis

(A) Modulation of AMPK pathway activity alters the formation of entotic structures. Graph shows number of entotic structures in MCF-7 cells grown in respective media with or without an AMPK inhibitor or two distinct activators, or MCF-7 cells expressing dominant-negative (DN) isoforms of AMPK (AMPKα1 and α2), for 72 hr, as determined by immunofluorescence. Shown are individual data points from independent experiments. Immunostaining for β-catenin (green) and Lamp1 (red) and DAPI-stained nuclei (blue) is shown. Arrow shows internalized cells, red arrowheads mark entotic corpses, and white arrowhead marks partial engulfment. Scale bar, 15 μm. See also Figures S3A–S3C.

(B) AMPK activity increases within internalizing cells during glucose starvation. Graph on the left shows normalized AMPKAR FRET ratio of internalizing cells ("inner cell") in glucose-free media throughout 12 hr (10 hr prior to completion of entosis and 2 hr after engulfment is complete, as determined by imaging), as well as AMPKAR values of entotic host cells ("outer cell") and neighboring single cells. Data are from two independent experiments (n = 10 and n = 12, respectively). p values according to two-way ANOVA multiple comparisons test. Graph on right shows FRET values of matched outer and inner cell pairs 1 hr before completion of engulfment. Images show representative entotic engulfment of cells expressing AMPKAR. The white dashed line marks the boundary between cells (inner cell is labeled by white arrow); the red dashed line marks an inner cell within an outer cell after entosis. Scale bar, 10 μm.

(C) Overexpression of DN AMPKα1 blocks loser cell behavior in MCF-7 cells cultured in glucose-free media. Graph shows quantification of heterotypic entotic structures of mCherry-expressing AMPKα1-DN cells cultured 1:1 with parental cells (expressing GFP) and cultured in glucose-free media for 72 hr. Error bars show mean ± SEM; data are from at least three independent experiments. See also Figures S3B and S3D.

(D) Overexpression of constitutively active Rac1^{V12} (Rac1^{CA}-GFP) blocks glucose starvation-induced entosis. Graph shows quantification of entosis events over 72 hr in parental MCF-7 cells or cells expressing constitutively active Rac1 grown in full or glucose-free media, as determined by time-lapse microscopy. Error bars show mean ± SEM; data are from at least three independent experiments. Time-lapse images show cells expressing Rac1^{CA}-GFP. Time shown is in hours:minutes. Scale bars, 15 μm.

have shown previously has loser cell activity. Long-term glucose starvation also selects for winner cell behavior that is associated with increased proliferation, changes in cell ploidy, and a long-term ability to grow in the absence of glucose.

DISCUSSION

Here, we find that nutrient deprivation in the form of glucose withdrawal is an inducer of the cell engulfment and death mechanism entosis. Thus, in addition to matrix detachment, metabolic stress resulting from insufficient glucose availability, which is known to occur during tumorigenesis (Denko, 2008), may induce entosis in human cancers. As entosis promotes the scavenging of nutrients by winner cells from losers, its induction in this context allows cell populations to respond to starvation stress, promoting competition between cells.

We find that glucose starvation induces entosis by activating the energy-sensing kinase AMPK within loser cells. Consistent with this, the activation of Rac1, which blocks loser cell behavior, inhibits starvation-induced entosis. Mechanical measurements of cells undergoing glucose starvation revealed the appearance of a bimodal population of cells consisting of one group that is much more deformable and a second group that is less deformable in a manner dependent on AMPK activity. These data support a model where glucose starvation activates entosis by upregulating loser cell behavior, which is known to be controlled by RhoA and ROCK. Long-term glucose withdrawal can lead to AMPK-dependent cell death by apoptosis (Okoshi et al., 2008;

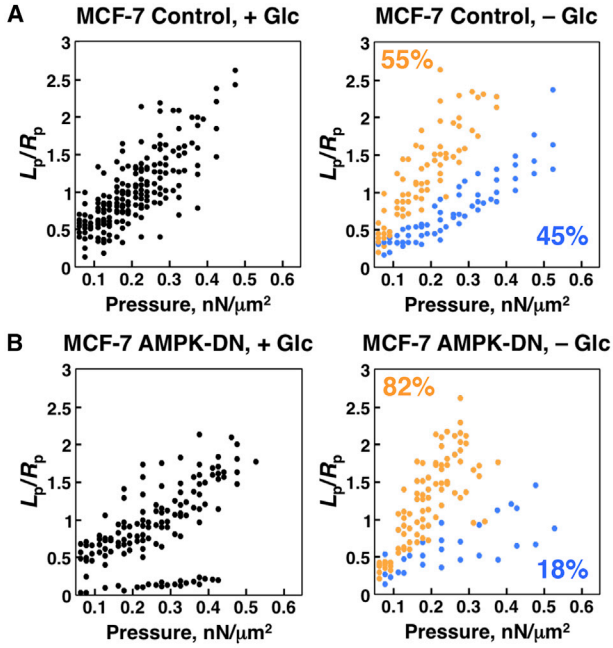

C

Cell type	Elastic Modulus (nN/μm²) mean ± SEM, *n*	*P*-value
MCF-7 Control, + Glc	0.050 ± 0.003, *39*	
MCF-7 Control, – Glc	0.039 ± 0.002, *12*	0.46
MCF-7 Control, – Glc	0.072 ± 0.007, *10*	0.038
MCF-7 AMPK-DN, + Glc (upper)	0.077 ± 0.005, *19*	
MCF-7 AMPK-DN, + Glc (lower)	0.498 ± 0.05, *4*	0.0005
MCF-7 AMPK-DN, – Glc	0.029 ± 0.001, *27*	0.0003
MCF-7 AMPK-DN, – Glc	0.151 ± 0.032, *6*	0.0004

Figure 4. Glucose Starvation Alters Cell Deformability in an AMPK-Dependent Manner

(A) Glucose starvation induces two mechanically distinct cell populations. The scatterplot on the left shows individual measurements of control MCF-7 cells cultured in full media conditions for 48 hr (+Glc). The scatterplot on the right shows control MCF-7 cells cultured in glucose-free media for 48 hr (−Glc). Note the appearance of two distinct populations upon glucose starvation. The y axis represents the deformation of individual cells (L_p) normalized by the radius of the micropipette (R_p). Cell measurements were color-coded based on each cell's degree of deformability at high pressures. The distribution of slopes for individual cells in both control and −Glc conditions were tested using the dip test for multimodality (R statistical package). The control dataset was consistent with a monomodal distribution (p = 0.854), while the −Glc dataset was consistent with a bimodal population distribution (p = 0.015).

(B) Expression of AMPK-DN blocks the appearance of less-deformable cell population in glucose starvation. On the left are individual measurements of MCF-7 cells expressing a DN isoform of AMPK (AMPK-DN) grown in full media for 48 hr. On the right are individual measurements of AMPK-DN cells grown in glucose-free conditions for 48 hr. The number of cells present in the blue, less deformable category in glucose starvation is significantly reduced by expression of AMPK-DN (compare to the −Glc graph in A).

(C) Summary of measured mechanical parameters. Font color corresponds to populations labeled in the same color in (A) and (B), respectively. p values listed for MCF-7 control, −Glc set were compared to MCF-7 control, +Glc cells; p values for MCF-7 AMPK-DN, −Glc were compared to MCF-7 AMPK-DN, +Glc (top) cells. p values were obtained by ANOVA with Fisher's least significant difference test.

El-Masry et al., 2012). Our data demonstrate that AMPK can also promote cell death through entosis, an effect potentially linked to the known AMPK-dependent control over myosin contractility (Thaiparambil et al., 2012; Bultot et al., 2009). Entosis may have the unique property of distributing nutrients to winner cells within a starved population, thereby supporting population regrowth following acute induction of cell death that initially reduces cell number. Intriguingly, we find that entosis inhibition by depletion of E-cadherin or treatment with Y-27632 increases rates of necrosis while having no effect on the overall death percentage (Figures 5B and 5C). Future studies to explore if this observed relationship results from co-regulation of these mechanisms will be informative.

In addition to AMPK-dependent regulation of loser cell mechanics, about half of the cells in the population show increased deformability compared to controls (see Figure 4A). This highly deformable population becomes the dominant population upon AMPK inhibition (Figure 4B). Thus, glucose starvation triggers two events: high levels of AMPK activation in one population, leading to low deformability, and increased deformability in the other population, promoting winner status. In cells cultured in nutrient-replete medium, we have found that activators of AMPK (AICAR and A-769662) are sufficient to induce entosis, but less effectively than glucose starvation, suggesting that winner cell mechanics induced in starved cultures could contribute significantly to entosis induction. How glucose starvation promotes winner cell mechanics, as well as entotic cell death, and whether these activities could be coupled are important questions for further study.

Overall, we show that entosis is induced by glucose starvation and promotes competition between cancer cells. In addition to starvation responses, such as autophagy, which promotes nutrient recycling to support cell survival (Mizushima et al., 2008), and macropinocytosis, which allows cancer cells to scavenge extracellular protein to support proliferation (Commisso et al., 2013; Palm et al., 2015), entosis may be an important mechanism utilized by cancer cell populations to support metabolism under conditions of limiting nutrient availability. In the long-term, some cancer cells may also activate gluconeogenesis to adapt to the continual absence of glucose, as reported previously (Méndez-Lucas et al., 2014). We previously found that entosis disrupts cell ploidy, and we show here that starving cell populations exhibit multinucleation, suggesting that an additional consequence of engaging this mechanism may be to promote tumorigenesis through the promotion of gross aneuploidy. Dying cells have been shown to provide nutrients to support the survival and proliferation of neighboring cells in single-cell yeast and bacterial populations undergoing starvation (Gourlay et al., 2006; Fabrizio et al., 2004; Büttner et al., 2006). Our data suggest that some cancer cell populations may also respond to starvation by redistributing nutrients in a manner that maintains the proliferation of selected cells.

EXPERIMENTAL PROCEDURES

Cell Culture and Reagents

MCF-7 cells (Lombardi Cancer Center, Georgetown University, Washington, DC) were cultured in DMEM (11965-092; Life Technologies) supplemented with 10% heat-inactivated fetal bovine serum (FBS) (F2442; Sigma-Aldrich)

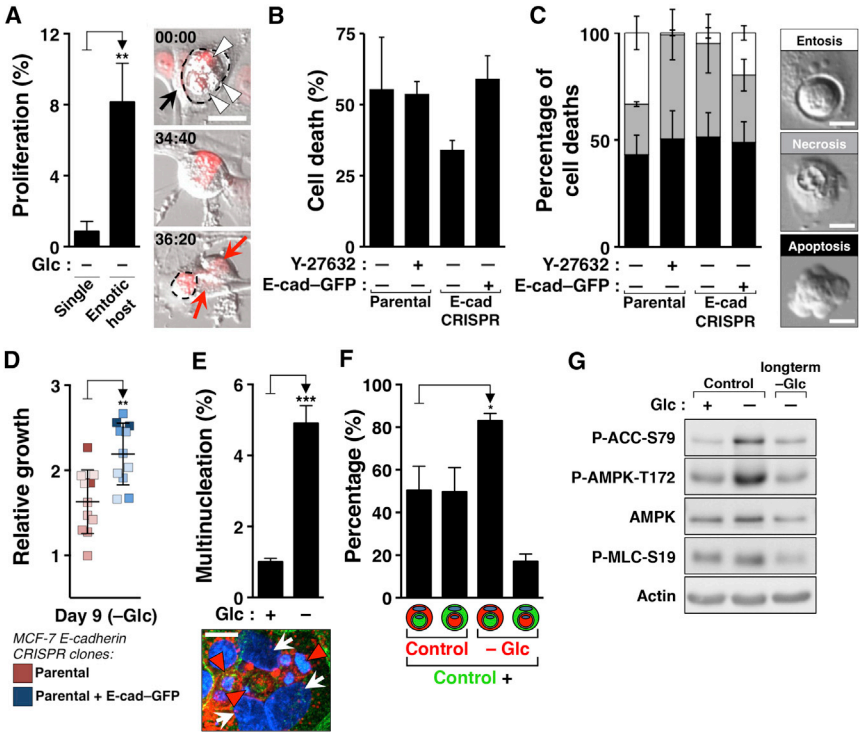

Figure 5. Consequences of Starvation-Induced Entosis

(A) Entotic host cells have a proliferative advantage in starvation conditions compared to non-engulfing single cells. Graph shows quantification of proliferation events of single and entotic host cells in glucose/amino acid-free media, imaged by time-lapse microscopy over 72 hr after an initial starvation period. Error bars show mean ± SEM; data are from at least three independent experiments. Images show entotic host cell (black arrow) with three engulfed corpses (arrowheads) in glucose/amino acid-free media undergoing cell division; red arrows mark two daughter cells. Time shown is in hours:minutes. Scale bar, 15 μm. See also Figure S4A.

(B) Inhibition of entosis does not increase overall rates of cell death. Graph shows quantification of all types of cell death in MCF-7 cells over 72 hr of glucose starvation, as determined by time-lapse microscopy. Error bars show mean ± SEM; data are from at least three independent experiments.

(C) Inhibition of entosis results in increased rates of necrotic cell death. Graph shows percentage of different types of cell death observed over 72 hr of glucose starvation by time-lapse microscopy. Error bars show mean ± SEM; data are from at least three independent experiments. Representative DIC images show the three types of death morphologies used to score cell death. Scale bars, 10 μm.

(D) Entosis-competent cells proliferate more than entosis-deficient cells in glucose-free conditions. Scatterplot shows the number of MCF-7 E-cad CRISPR (red) and E-cad CRISPR + E-cad-GFP cells (blue) after 9 days of glucose starvation relative to the cell number after 72 hr. Shown are individual values from three independent experiments (data points from experimental replicates are shaded accordingly). Error bars show mean ± SD.

(E) Glucose starvation induces multinucleation in MCF-7 cells. Graph shows quantification of multinucleated cells in cultures of MCF-7 cells grown in the presence or absence of glucose for 72 hr, as determined by immunofluorescence. Error bars show mean ± SEM; data are from at least three independent experiments. Image shows appearance of multinucleated cell after 72 hr of glucose starvation, with three nuclei (arrows) and three engulfed cells (arrowheads). Immunostaining for β-catenin (green) and Lamp1 (red) and DAPI-stained nuclei (blue) is shown. Scale bar, 10 μm. See also Figure S4B.

(F) Cells cultured under prolonged glucose starvation preferentially internalize parental cells. Graph shows the percentage of red-labeled cells (either parental MCF-7 or MCF-7 cells grown for 36–78 days in glucose-free conditions) that are hosts or internalized cells when mixed with passage-matched, green-labeled parental MCF-7 cells and cultured in glucose-free conditions for 72 hr. Error bars show mean ± SEM; data are from at least three independent experiments.

(G) AMPK and myosin activity is reduced in long-term glucose-starved cells. Western blot shows activation of AMPK and downstream signaling, as well as activation of myosin light chain, in MCF-7 cells cultured in the indicated conditions.

and penicillin/streptomycin (30-002-CI; Mediatech). MDA-MB-231 cells and its derivative were grown in RPMI (11875-093; Life Technologies) supplemented with 10% heat-inactivated FBS with penicillin/streptomycin, as described previously (Sun et al., 2014a). MCF-10A cells were cultured in DMEM/F-12 (11320-033; Life Technologies) supplemented with 5% horse serum (HS) (S12150; Atlanta Biologicals), 20 ng/mL epidermal growth factor (EGF) (AF-100-15; Peprotech), 10 μg/mL insulin (I-1882; Sigma-Aldrich), 0.5 μg/mL hydrocortisone (H-0888; Sigma-Aldrich), 100 ng/mL cholera toxin (C-8052; Sigma-Aldrich), and penicillin/streptomycin (30-002-CI; Mediatech), as previously described (Debnath et al., 2003). Glucose-free, amino acid-free, and glucose/amino acid-free medium was prepared by dialyzing heat-inactivated FBS for 4 hr at 4°C in PBS (P3813; Sigma-Aldrich) in MWCO 3500 dialysis tubing (21-152-9; Fisherbrand), followed by overnight at 4°C in fresh PBS and subsequent addition to base media prepared without respective component (glucose, amino acids, or glucose and amino acids, respectively) to a 10% final concentration. Cells expressing the H2B-mCherry nuclear marker were prepared by transducing cells with retroviruses made with the pBabe-H2B-mCherry construct, as described previously (Florey et al., 2011). The mCherry-AMPK-DN construct was generated by inserting the AMPKα2 K45R gene (from Plasmid #15992; Addgene) into the pQCXIP-mCherry retroviral vector. pEGFP-Rac1^{CA} was a gift from Dr. Alan Hall (Memorial Sloan Kettering Cancer Center, New York, NY). For disruption of E-cadherin in MCF-7 cells by CRISPR-Cas9, guide RNAs (gRNAs) were designed using the online CRISPR design tool from Feng Zhang's laboratory (http://crispr.mit.edu), and the gRNA with one of the highest theoretical mutagenic efficiencies was used (5′-CGCCGAGAGCTACACGTTCACGG-3′). The vector encoding for Cas9 (pCDNA3.3-TOPO-hCas9, plasmid #41815; Addgene), as well as vector encoding the gRNA (pCR-Blunt II-TOPO, plasmid #41824; Addgene), were introduced into control MCF-7 cells by nucleofection (Cell Line Nucleofector Kit V, VCA-1003; Lonza). Single-cell clones were selected and examined for disruption of E-cadherin by sequencing and western blotting. Cells were treated with Y-27632 (#1254; Tocris Bioscience) at 10 μM, AICAR (#9944; Cell Signaling Technology) at 2 mM, A-769662 at 500 nM (#3336; Tocris Bioscience), and compound C (P5499; Sigma-Aldrich) at 10 μM. Inhibitors (or vehicle) were added to cultures ~30 min before the start of biological assays unless indicated otherwise.

Western Blotting

Cells were lysed in ice-cold RIPA buffer and western blotting was performed as described previously (Florey et al., 2011). The following antibodies were used: anti-E-cadherin (1:500; 3195, Cell Signal), anti-tubulin (1:2,000; 3873, Cell Signal), anti-Atg5 (1:500; 2630, Cell Signal), anti-phospho-ACC-S79 (1:500; 3661, Cell Signal), anti-ACC (1:500; 3662, Cell Signal), anti-phospho-AMPK-T172 (1:500; 2531, Cell Signaling), anti-mCherry (1:500; ab125096, Abcam),

anti-β-actin (1:2000; A1978, Sigma-Aldrich), anti-rabbit immunoglobulin G (IgG) horseradish peroxidase (HRP)-linked antibody (1:5,000; 7074, Cell Signal), and anti-mouse IgG HRP-linked antibody (1:5,000; 7076, Cell Signal).

Immunofluorescence

The following antibodies were used for immunofluorescence (IF): anti-β-catenin (1:100; C2206; Sigma-Aldrich), anti-Lamp1 (1:100; 555798; BD Biosciences), Alexa Fluor 568 goat anti-mouse secondary (1:500; A-11031; Life Technologies), and Alexa Fluor 488 goat anti-rabbit secondary (1:500; A-11034; Life Technologies). IF was performed on cells cultured on glass-bottom dishes (P35G-1.5-20-C; MatTek), as described previously (Overholtzer et al., 2007). Briefly, cells were fixed in 1:1 methanol/acetone for 5 min at −20°C, followed by three 5-min PBS washes and blocking in 5% BSA, 100 mM glycine in PBS for 1 hr, followed by incubation with primary antibodies at 4°C overnight. Samples were then incubated with secondary antibodies and counterstained with DAPI (1:1,000; D1306; Life Technologies). Confocal microscopy was performed with the Ultraview Vox spinning-disk confocal system (PerkinElmer) equipped with a Yokogawa CSU-X1 spinning-disk head and an electron-multiplying charge-coupled device camera (Hamamatsu C9100-13) coupled to a Nikon Ti-E microscope; image analysis was done using Volocity software (PerkinElmer).

Time-Lapse Microscopy

Cells were cultured on glass-bottom dishes (P06G-1.5-20-F; MatTek), and time-lapse microscopy was performed in 37°C and 5% CO_2 live-cell incubation chambers, as described previously (Florey et al., 2011). Fluorescence and differential interference contrast (DIC) images were acquired every 20 min for 72 hr using a Nikon Ti-E inverted microscope attached to a CoolSNAP charge-coupled device camera (Photometrics) and NIS Elements software (Nikon). For tetramethylrhodamine, ethyl ester, perchlorate (TMRE) imaging, TMRE (T669; Thermo Fisher Scientific) was added to cultures to be imaged at a final concentration of 100 nM.

Entosis Quantification

For quantification of entosis in MCF-7 cells by immunofluorescence, 250,000 cells were plated on 35-mm glass-bottom dishes and allowed to adhere overnight, washed briefly three times with PBS, cultured in the indicated conditions for 72 hr, and fixed and stained as described above. The percentage of entotic cells was determined by counting at least 300 cells in each sample and quantifying the number of single cells and cell-in-cell structures; both dead (LAMP1-positive compartments) and live cells were counted as entotic. If one host cell contained two cells in separate compartments, it was scored as two engulfment events. In sequential cell-in-cell structures (see Figures 1Ai and 1Aii), only the outermost cell was counted as an entotic host. Fold induction of entosis in MCF-7 and MDA-MB-231 cells by time-lapse microscopy was determined as follows: engulfment events were scored by the appearance of a vacuole within the host cell throughout 72 hr and normalized to cell number at time 0 hr; normalized engulfment numbers from all conditions were then normalized to full media conditions ("fold induction"). For fate of internalized cells, time 0 of engulfment was determined by the appearance of a host cell vacuole; cell death was scored by changes in cell morphology in the DIC channel. For quantification of entosis in MCF-10A cells by immunofluorescence, 500,000 cells were plated on 60-mm tissue culture dishes (353002; Corning) and allowed to adhere overnight, washed briefly three times with PBS, and cultured in the indicated media for 96 hr (media was replaced after 48 hr). After 96 hr, cells were trypsinized (25053CI; Corning) to achieve a single-cell suspension, and 250,000 cells were re-plated on 35-mm glass-bottom dishes in fresh media (either full or glucose-free) and allowed to adhere for 12 hr (for a total of 108 hr of starvation), at which point cells were fixed and stained as described above.

AMPK FRET Measurements

A modified version of the AMPK activity reporter (AMPKAR) (Tsou et al., 2011) with an extended "EV" linker (Komatsu et al., 2011) was stably integrated into MCF-7 cells using PiggyBac transposase. Homogeneous populations of reporter-expressing cells were isolated by limited dilution cloning; three independent clones were analyzed. Time-lapse imaging was performed as previously described (Sparta et al., 2015) using a Nikon TiE with a 20× 0.75 NA Plan-Apochromat objective and CFP and YFP filter cubes (Chroma 49001 and 49003, respectively). Images were recorded with an Andor Zyla scMOS camera, using Nikon Elements software. For imaging, cells were plated on #1.5 glass-bottom 96-well plates (P96-1.5H-N; In Vitro Scientific) and maintained at 37°C and 5% CO_2. Raw image files were imported to ImageJ, where tracking of cells and measurement of fluorescence values was performed manually using a modified version of the "Manual Tracking" plugin. AMPKAR signals were calculated as the average background-subtracted CFP/YFP ratio within three 3-by-3-pixel regions of the cytoplasm.

MPA Assay

MPA was performed as described previously (Sun et al., 2014b; Zhou et al., 2010). In short, after culturing cells in either full or glucose-free media for 48 hr, cells were trypsinized, pelleted by spinning down for 5 min at 1,500 × *g*, and re-suspended in the appropriate media. Prior to being measured, the cells were incubated for 15 min at 37°C and 5% CO_2. Cells were aspirated with 6- to 8-μm pipettes at varying and increasing pressures. For data analysis, the length of the deformation of the cell cortex pulled into the micropipette (L_p) was divided by the radius of the pipette (R_p), and L_p/R_p values were plotted as a function of applied pressure. These data were converted into apparent elastic moduli (Hochmuth, 2000). The distribution of slopes for individual cells in both the control and the −Glc conditions were tested using the dip test for multimodality (R statistical package), and the resulting subpopulations were analyzed using ANOVA with Fisher's least significant difference test.

Proliferation Advantage Assay

250,000 cells per 35-mm well were plated on glass and allowed to adhere overnight. Cells were washed in PBS three times and grown in glucose/amino acid-free media for 72 hr to induce entosis. After, cells were washed in PBS and either full or glucose/amino acid-free media containing 10 μM Y-27632 was added to cells to inhibit further cell engulfment; cells were then imaged for 72 hr at 20-min intervals. Cell fates of entotic hosts or single cells in each field of view were determined throughout this time.

Population Growth Assay

100,000 cells were seeded in triplicate in 12-well culture dishes (#3512; Corning) and allowed to adhere overnight. Cells were washed in PBS three times and grown in glucose-free media for 9 days, with three PBS washes and media replacement every 72 hr. For crystal violet staining, cells were washed once in PBS, fixed in 4% paraformaldehyde (PFA) in PBS for 15 min, washed once with H_2O, and subsequently stained with 0.1% crystal violet solution (in 10% ethanol) for 20 min. Crystal violet solution was aspirated, and cells were washed three times with H_2O and allowed to air-dry overnight. The following day, crystal violet was extracted by incubating the cells with 1 mL 10% acetic acid for 20 min with gentle shaking, followed by absorbance measurements at 570 nm. Values were normalized to respective absorbance at day 3 of glucose starvation.

Quantification of Winner and Loser Cell Identity

Passage-matched cells (either control MCF-7 or −Glc MCF-7 (starved for glucose for 36–78 days with change of media every 3 days) were labeled with 10 μM CellTracker dyes (green or red, C7025 and C34552, respectively; Life Technologies) for 20 min at 37°C and then plated at a 1:1 ratio at a total cell density of 250,000 cells in 35-mm glass-bottom dishes overnight in media containing 10 μM Y-27632 to block entosis. The next day, cells were washed three times with PBS and glucose-free media was added for 72 hr, at which point cells were analyzed by confocal microscopy. Heterotypic cell-in-cell structures were counted and the number of structures of green-inside-red and red-inside-green determined. For competition assays with AMPKα1 DN cells, stable mCherry-expressing MCF-7 cells were transfected (using Amaxa Nucleofector, VCA-1003; Lonza) according to the manufacturer's protocol) with either a vector expressing AMPK α1 DN (K47R) (plasmid #79011; Addgene) or empty vector and allowed to recover overnight. Cells were then mixed at a 1:1 ratio with stable GFP-expressing MCF-7 cells and plated and analyzed for cell-in-cell structures according to the same protocol described

above. For competition assays with AMPKα2 DN cells, MCF-7 cells stably expressing either mCherry (control) or mCherry-AMPKα2 K45R DN were mixed at a 1:1 ratio with stable GFP-expressing MCF-7 cells and plated and analyzed as described above.

Statistics

The indicated p values were obtained using Student's t test unless otherwise noted (***, $p < 0.001$; **, $p < 0.01$; *, $p < 0.05$; n.s., not significant).

SUPPLEMENTAL INFORMATION

Supplemental Information contains four figures and can be found with this article online at http://dx.doi.org/10.1016/j.celrep.2017.06.037.

AUTHOR CONTRIBUTIONS

J.C.H. and M.O. designed and carried out experiments and wrote the paper. D.N.R. and A.S. designed, performed, and analyzed the MPA experiments and participated in writing the paper. J.G.A. and C.T. designed, performed, and analyzed the AMPKAR FRET experiments. R.C. generated CRISPR knockout cell lines. All authors participated in editing the manuscript.

ACKNOWLEDGMENTS

This work was supported by NIH grants CA154649 (to M.O.) and GM66817 (to D.N.R.) and the Benjamin Friedman Research Fund (to M.O.). We thank members of the Overholtzer lab for critical reading of the manuscript and Jennifer Nguyen and Pablo Iglesias (Johns Hopkins University School of Medicine) for help with statistical analysis of MPA data.

Received: September 9, 2016
Revised: May 5, 2017
Accepted: June 13, 2017
Published: July 5, 2017

REFERENCES

Banko, M.R., Allen, J.J., Schaffer, B.E., Wilker, E.W., Tsou, P., White, J.L., Villén, J., Wang, B., Kim, S.R., Sakamoto, K., et al. (2011). Chemical genetic screen for AMPKα2 substrates uncovers a network of proteins involved in mitosis. Mol. Cell *44*, 878–892.

Bultot, L., Horman, S., Neumann, D., Walsh, M.P., Hue, L., and Rider, M.H. (2009). Myosin light chains are not a physiological substrate of AMPK in the control of cell structure changes. FEBS Lett. *583*, 25–28.

Büttner, S., Eisenberg, T., Herker, E., Carmona-Gutierrez, D., Kroemer, G., and Madeo, F. (2006). Why yeast cells can undergo apoptosis: death in times of peace, love, and war. J. Cell Biol. *175*, 521–525.

Commisso, C., Davidson, S.M., Soydaner-Azeloglu, R.G., Parker, S.J., Kamphorst, J.J., Hackett, S., Grabocka, E., Nofal, M., Drebin, J.A., Thompson, C.B., et al. (2013). Macropinocytosis of protein is an amino acid supply route in Ras-transformed cells. Nature *497*, 633–637.

Debnath, J., Muthuswamy, S.K., and Brugge, J.S. (2003). Morphogenesis and oncogenesis of MCF-10A mammary epithelial acini grown in three-dimensional basement membrane cultures. Methods *30*, 256–268.

Degterev, A., Huang, Z., Boyce, M., Li, Y., Jagtap, P., Mizushima, N., Cuny, G.D., Mitchison, T.J., Moskowitz, M.A., and Yuan, J. (2005). Chemical inhibitor of nonapoptotic cell death with therapeutic potential for ischemic brain injury. Nat. Chem. Biol. *1*, 112–119.

Denko, N.C. (2008). Hypoxia, HIF1 and glucose metabolism in the solid tumour. Nat. Rev. Cancer *8*, 705–713.

Dixon, S.J., Lemberg, K.M., Lamprecht, M.R., Skouta, R., Zaitsev, E.M., Gleason, C.E., Patel, D.N., Bauer, A.J., Cantley, A.M., Yang, W.S., et al. (2012). Ferroptosis: an iron-dependent form of nonapoptotic cell death. Cell *149*, 1060–1072.

El-Masry, O.S., Brown, B.L., and Dobson, P.R. (2012). Effects of activation of AMPK on human breast cancer cell lines with different genetic backgrounds. Oncol. Lett. *3*, 224–228.

Fabrizio, P., Battistella, L., Vardavas, R., Gattazzo, C., Liou, L.L., Diaspro, A., Dossen, J.W., Gralla, E.B., and Longo, V.D. (2004). Superoxide is a mediator of an altruistic aging program in Saccharomyces cerevisiae. J. Cell Biol. *166*, 1055–1067.

Florey, O., Kim, S.E., Sandoval, C.P., Haynes, C.M., and Overholtzer, M. (2011). Autophagy machinery mediates macroendocytic processing and entotic cell death by targeting single membranes. Nat. Cell Biol. *13*, 1335–1343.

Galluzzi, L., Vitale, I., Abrams, J.M., Alnemri, E.S., Baehrecke, E.H., Blagosklonny, M.V., Dawson, T.M., Dawson, V.L., El-Deiry, W.S., Fulda, S., et al. (2012). Molecular definitions of cell death subroutines: recommendations of the Nomenclature Committee on Cell Death 2012. Cell Death Differ. *19*, 107–120.

Gao, M., Monian, P., Quadri, N., Ramasamy, R., and Jiang, X. (2015). Glutaminolysis and transferrin regulate ferroptosis. Mol. Cell *59*, 298–308.

Göransson, O., McBride, A., Hawley, S.A., Ross, F.A., Shpiro, N., Foretz, M., Viollet, B., Hardie, D.G., and Sakamoto, K. (2007). Mechanism of action of A-769662, a valuable tool for activation of AMP-activated protein kinase. J. Biol. Chem. *282*, 32549–32560.

Gourlay, C.W., Du, W., and Ayscough, K.R. (2006). Apoptosis in yeast—mechanisms and benefits to a unicellular organism. Mol. Microbiol. *62*, 1515–1521.

Hochmuth, R.M. (2000). Micropipette aspiration of living cells. J. Biomech. *33*, 15–22.

Komatsu, N., Aoki, K., Yamada, M., Yukinaga, H., Fujita, Y., Kamioka, Y., and Matsuda, M. (2011). Development of an optimized backbone of FRET biosensors for kinases and GTPases. Mol. Biol. Cell *22*, 4647–4656.

Krajcovic, M., Johnson, N.B., Sun, Q., Normand, G., Hoover, N., Yao, E., Richardson, A.L., King, R.W., Cibas, E.S., Schnitt, S.J., et al. (2011). A non-genetic route to aneuploidy in human cancers. Nat. Cell Biol. *13*, 324–330.

Krajcovic, M., Krishna, S., Akkari, L., Joyce, J.A., and Overholtzer, M. (2013). mTOR regulates phagosome and entotic vacuole fission. Mol. Biol. Cell *24*, 3736–3745.

Linkermann, A., and Green, D.R. (2014). Necroptosis. N. Engl. J. Med. *370*, 455–465.

Liu, Y., Shoji-Kawata, S., Sumpter, R.M., Jr., Wei, Y., Ginet, V., Zhang, L., Posner, B., Tran, K.A., Green, D.R., Xavier, R.J., et al. (2013). Autosis is a Na+,K+-ATPase-regulated form of cell death triggered by autophagy-inducing peptides, starvation, and hypoxia-ischemia. Proc. Natl. Acad. Sci. USA *110*, 20364–20371.

Méndez-Lucas, A., Hyroššová, P., Novellasdemunt, L., Viñals, F., and Perales, J.C. (2014). Mitochondrial phosphoenolpyruvate carboxykinase (PEPCK-M) is a pro-survival, endoplasmic reticulum (ER) stress response gene involved in tumor cell adaptation to nutrient availability. J. Biol. Chem. *289*, 22090–22102.

Mizushima, N., Levine, B., Cuervo, A.M., and Klionsky, D.J. (2008). Autophagy fights disease through cellular self-digestion. Nature *451*, 1069–1075.

Mu, J., Brozinick, J.T., Jr., Valladares, O., Bucan, M., and Birnbaum, M.J. (2001). A role for AMP-activated protein kinase in contraction- and hypoxia-regulated glucose transport in skeletal muscle. Mol. Cell *7*, 1085–1094.

Nelson, C., Ambros, V., and Baehrecke, E.H. (2014). miR-14 regulates autophagy during developmental cell death by targeting ip3-kinase 2. Mol. Cell *56*, 376–388.

Okoshi, R., Ozaki, T., Yamamoto, H., Ando, K., Koida, N., Ono, S., Koda, T., Kamijo, T., Nakagawara, A., and Kizaki, H. (2008). Activation of AMP-activated protein kinase induces p53-dependent apoptotic cell death in response to energetic stress. J. Biol. Chem. *283*, 3979–3987.

Overholtzer, M., Mailleux, A.A., Mouneimne, G., Normand, G., Schnitt, S.J., King, R.W., Cibas, E.S., and Brugge, J.S. (2007). A nonapoptotic cell death process, entosis, that occurs by cell-in-cell invasion. Cell *131*, 966–979.

Palm, W., Park, Y., Wright, K., Pavlova, N.N., Tuveson, D.A., and Thompson, C.B. (2015). The utilization of extracellular proteins as nutrients is suppressed by mTORC1. Cell *162*, 259–270.

Sparta, B., Pargett, M., Minguet, M., Distor, K., Bell, G., and Albeck, J.G. (2015). Receptor level mechanisms are required for epidermal growth factor (EGF)-stimulated extracellular signal-regulated kinase (ERK) activity pulses. J. Biol. Chem. *290*, 24784–24792.

Sullivan, J.E., Carey, F., Carling, D., and Beri, R.K. (1994). Characterisation of 5′-AMP-activated protein kinase in human liver using specific peptide substrates and the effects of 5′-AMP analogues on enzyme activity. Biochem. Biophys. Res. Commun. *200*, 1551–1556.

Sun, Q., Cibas, E.S., Huang, H., Hodgson, L., and Overholtzer, M. (2014a). Induction of entosis by epithelial cadherin expression. Cell Res. *24*, 1288–1298.

Sun, Q., Luo, T., Ren, Y., Florey, O., Shirasawa, S., Sasazuki, T., Robinson, D.N., and Overholtzer, M. (2014b). Competition between human cells by entosis. Cell Res. *24*, 1299–1310.

Thaiparambil, J.T., Eggers, C.M., and Marcus, A.I. (2012). AMPK regulates mitotic spindle orientation through phosphorylation of myosin regulatory light chain. Mol. Cell. Biol. *32*, 3203–3217.

Tsou, P., Zheng, B., Hsu, C.H., Sasaki, A.T., and Cantley, L.C. (2011). A fluorescent reporter of AMPK activity and cellular energy stress. Cell Metab. *13*, 476–486.

Young, N.P., Kamireddy, A., Van Nostrand, J.L., Eichner, L.J., Shokhirev, M.N., Dayn, Y., and Shaw, R.J. (2016). AMPK governs lineage specification through Tfeb-dependent regulation of lysosomes. Genes Dev. *30*, 535–552.

Yuan, H.X., Xiong, Y., and Guan, K.L. (2013). Nutrient sensing, metabolism, and cell growth control. Mol. Cell *49*, 379–387.

Zhou, G., Myers, R., Li, Y., Chen, Y., Shen, X., Fenyk-Melody, J., Wu, M., Ventre, J., Doebber, T., Fujii, N., et al. (2001). Role of AMP-activated protein kinase in mechanism of metformin action. J. Clin. Invest. *108*, 1167–1174.

Zhou, Q., Kee, Y.S., Poirier, C.C., Jelinek, C., Osborne, J., Divi, S., Surcel, A., Will, M.E., Eggert, U.S., Müller-Taubenberger, A., et al. (2010). 14-3-3 coordinates microtubules, Rac, and myosin II to control cell mechanics and cytokinesis. Curr. Biol. *20*, 1881–1889.